The Influence of Defects on the Luminescence of Trivalent Terbium in Nanocrystalline Yttrium Orthovanadate

Journal:	*Nano Letters*
Manuscript ID	nl-2021-04937r.R2
Manuscript Type:	Communication
Date Submitted by the Author:	12-Apr-2022
Complete List of Authors:	Perrella, Rafael; Universidade Estadual de Campinas, Inorganic Chemistry Walker, Marc; University of Warwick, Department of Physics Chamberlain, Thomas; University of Warwick, Department of Chemistry Walton, Richard; University of Warwick, Department of Chemistry de Sousa Filho, Paulo; Universidade Estadual de Campinas Instituto de Quimica, Inorganic Chemistry

The Influence of Defects on the Luminescence of Trivalent Terbium in Nanocrystalline Yttrium Orthovanadate

Rafael Vieira Perrella,[†] Marc Walker,[§] Thomas William Chamberlain,[‡] Richard I. Walton,[‡]

Paulo Cesar de Sousa Filho[†,*]

[†]Department of Inorganic Chemistry, Institute of Chemistry, University of Campinas (Unicamp), R. Monteiro Lobato, 270, 13083-970, Campinas, São Paulo, Brazil

[§]Department of Physics, University of Warwick, Coventry, CV4 7AL, United Kingdom

[‡]Department of Chemistry, University of Warwick, Gibbet Hill Road, Coventry CV4 7AL, United Kingdom

*Corresponding author: pcsfilho@unicamp.br

ABSTRACT: Terbium-doped YVO_4 has been considered a non-luminescent solid since the first classic studies on rare-earth-doped phosphors in the 1960s. However, we demonstrate that defect engineering of $YVO_4:Tb^{3+}$ nanoparticles overcomes the metal-metal charge transfer (MMCT) process which is responsible for the quenching of the Tb^{3+} luminescence. Tetragonal $(Y_{1-x}Tb_x)VO_4$ nanoparticles obtained by colloidal precipitation showed expanded unit cells, high defect densities, and intimately mixed carbonates and hydroxides, which contribute to a shift of the MMCT states to higher energies. Consequently, we demonstrate unambiguously for the first time that Tb^{3+} luminescence can be excited by $VO_4^{3-} \rightarrow Tb^{3+}$ energy transfer and by direct population of the $^5D_4$ state in YVO_4. We also discuss how thermal treatment removes these effects and shifts the quenching MMCT state to lower energies, thus highlighting the major consequences of defect density and microstructure in nanosized phosphors. Therefore, our findings ultimately show nanostructured $YVO_4:Tb^{3+}$can be reclassified as a UV-excitable luminescent material.

KEYWORDS vanadates; terbium; rare-earth; luminescence; nanoparticles; colloidal coprecipitation.

Luminescent rare-earth (RE) oxides have been extensively explored both in terms of theoretical detailing of 4*f*-4*f* transitions and for their unique applicability in lighting, visualization, non-linear optics, and biolabeling technologies.[1-6] RE vanadates ($REVO_4$) are chemically stable and remarkably versatile hosts for lanthanoid (Ln) optical centers with downshift and upconversion emissions, which enable emerging applications in nanothermometry, sensing, and catalysis.[7-9] Whilst Eu^{3+}-doped YVO_4 is an ubiquitous UV-excited red phosphor,[1,5,6,9] the inactivity of Tb^{3+}-doped YVO_4 is an intriguing aspect in the chemistry and spectroscopy of vanadate-based luminescent materials.[6,10,11] During the search for efficient lamp phosphors in the late 1960s, many groups reported the complete absence of Tb^{3+} luminescence in YVO_4 as well as the strong quenching of other Ln^{3+} emissions induced by Tb^{3+}-codoping.[11-15] Even though some groups studied Tb^{3+} emissions in lanthanum ($LaVO_4$)[16-21] or gadolinium ($GdVO_4$)[20-22] vanadates, papers mentioning any luminescence in tetragonal YVO_4:Tb^{3+} are scarce,[12,21,23,24] and no spectra or detailed characterization have been reported. The description of the Tb^{3+} luminescence in AXO_4 zircon-type solids has been mainly performed for yttrium phosphates (YPO_4), phosphovanadates ($YP_{1-x}V_xO_4$), and arsenovanadates ($YAs_{1-x}V_xO_4$), which are isostructural to YVO_4.[6,25-27]

The absence of Tb^{3+} luminescence in YVO_4 was initially explained by an inefficient $VO_4^{3-} \rightarrow Tb^{3+}$ energy transfer process, but further observation and the pivotal works of Blasse[28-30] and DeLosh[25] suggested that the luminescence quenching stems from low-lying metal-metal charge transfer (MMCT) states. Such states are also termed as intervalence charge transfer (IVCT) processes,[31] in which a $Tb^{3+} \rightarrow V^{5+}$ electron transfer results in an approximate $Tb^{\bullet}_{Tb}$-V'_V transient charge distribution, interpreted as a Tb^{4+}/V^{4+} couple. Different works[20,29,31] proposed that the

quenching rates are reduced when MMCT states are shifted to higher energies, which could be achieved by increasing the positive charge density on the Tb^{3+} sites or increasing the electron density of the transition metal center. This has been confirmed by the observation of $VO_4^{3-} \rightarrow Tb^{3+}$ energy transfer in aliovalent-substituted $CaSO_4:V^{5+},Tb^{3+}$.[29] Likewise, Tb^{3+} emission intensities in $YXO_4:Tb^{3+}$ solids (X=V, Nb, or Ta) become detectable and stronger with decreasing 5th ionization energies of the transition metal [in kJ mol^{-1}: 6299 (V)> 4880 (Nb)> 4658 (Ta)], also supporting this proposition.[30] However, the MMCT state has not been probed systematically for Tb^{3+} in tetragonal YVO_4, and no evidence of the possibility of tuning the position of this state via modifications other than substitution of the pentavalent element has been demonstrated to date. This would be highly interesting for selective activation/deactivation of Tb^{3+} luminescence for sensing purposes, for instance.[32]

The synthetic methodology has not generally been considered in the investigation of the Tb^{3+} inactivity in YVO_4. The classic literature concerning this solid mostly comprises materials prepared by conventional solid-state syntheses[11-15] or coprecipitations[18] followed by high temperature annealing.[23] Solid-state methods not only may lead to incomplete reaction of precursors, and eventually to misleading conclusions (*i.e.*, observation of luminescence due to residual oxides),[12,24] but also the high temperature conditions inevitably cause irreversible aggregation of particles, and crystallite growth. Structural and compositional nanoscale effects on the luminescence of Tb^{3+} in YVO_4 have not been discussed to the best of our knowledge. We herein demonstrate that Tb^{3+} shows surprisingly intense luminescence in pristine YVO_4 nanoparticles produced by colloidal synthesis even at high doping concentrations (*ca.* 40%) or after moderate (<500 °C) thermal treatments.

Details about the synthesis[8,33-37] of the $Y_{1-x}Tb_xVO_4$ particles and general characterization (Fig. 1) are discussed in the Supporting Information (Section 2, p.S6-S7). The strongly basic conditions in which particles were generated resulted in high amounts of non-crystalline hydroxides and carbonates[35,36] mixed in a very intimate level to the 30 nm tetragonal vanadate crystallites.

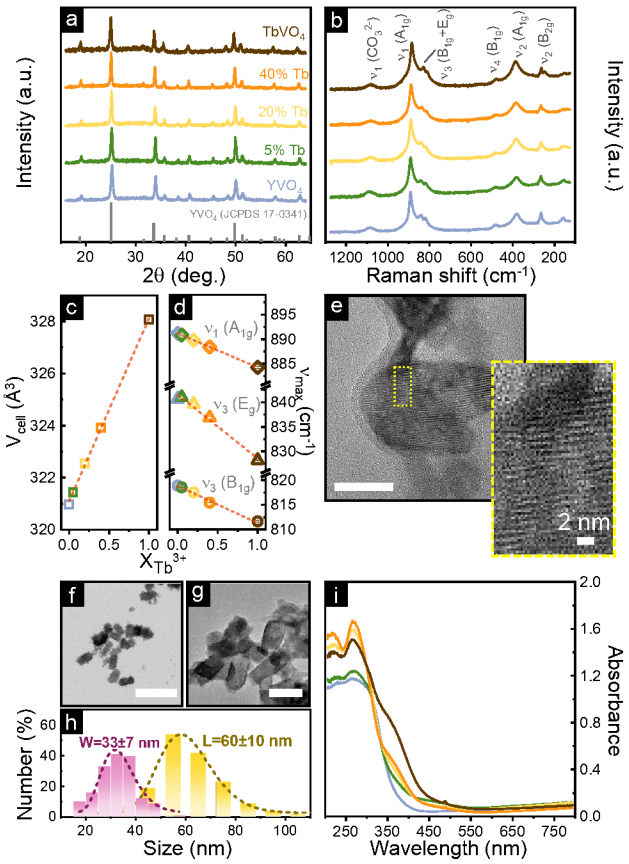

Figure 1. (a) Powder X-ray diffractograms, (b) Raman spectra, and (c,d) linear correlation between Tb^{3+} molar fractions ($x_{Tb^{3+}}$) and (c) cell volumes and (d) symmetric [ν_1 (A_{1g})] and antisymmetric [ν_3 (E_g + B_{1g})] stretching frequencies of the VO_4^{3-} group in the $Y_{1-x}Tb_xVO_4$ nanoparticles (x = 0, 0.05, 0.20, 0.40, and 1). Representative (e,f,g) transmission electron

microscopy images and (h) particle size distributions of $Y_{0.95}Tb_{0.05}VO_4$ nanoparticles. The scale bars in (e), (f) and (g) correspond to 20, 100 and 50 nm, respectively. (i) Room temperature UV-Vis absorption spectra of the $Y_{1-x}Tb_xVO_4$ nanoparticles. The color pattern in (a) is the same in (b), (c), (d) and (i).

We therefore conclude that the chemical composition of the particles showed a positive deviation of the RE:V molar ratio, and a general formula $RE(VO_4)_{1-0.66x-0.33y}(CO_3)_x(OH)_y$ better describes the solids obtained. Even though the presence of CO_3^{2-} and OH^- groups resulted in a non-stoichiometric RE:V molar ratio, these impurities resulted in minor adjustment of the oxidation states of V and Tb in the $Y_{1-x}Tb_xVO_4$ particles (Fig. 2). X-ray near edge absorption spectra (XANES) at the Tb L_{III} edge (Fig. 2a,b) demonstrated Tb^{3+} is the dominant terbium species both at low (5%) and intermediate (20%) concentrations, confirming ground state Tb^{4+} contribution is very low for the as-prepared $Y_{1-x}Tb_xVO_4$ particles (Fig S5). The position of the V pre-edge peak (K edge, Fig. 2d,e) is nearly identical for both Tb^{3+} concentrations (*i.e.* 5% and 20%) and suggests a mean oxidation state of 4.8 for V these solids. This agrees with the occurrence of partially reduced vanadium sites [*i.e.*, V'_V (V^{4+}) or V''_V (V^{3+})] that generally compensate surface and bulk oxygen vacancies ($v_O^{\cdot\cdot}$) and hydroxides ($OH_O^{\cdot}$). These reduced vanadium species were also probed by X-ray photoelectron spectroscopy (XPS, Fig. 2g-l), which showed broadened V2p signals due to the presence of V^{3+} and V^{4+} at the surface (Fig. 2i). In addition, the $Y3d_{5/2}$ and $3d_{3/2}$ signals are clearly doubled, and approximately 25% of the RE cation sites at the surface

are estimated to occur at the vicinity of oxygen vacancies (Fig. S6). XPS results also indicate a high deviation from the RE:V=1:1 stoichiometry at the surface, where an approximate RE:V ratio of 3.4:1 was found for $(Y_{0.95}Tb_{0.05})VO_4$, and $(Y_{0.60}Tb_{0.40})VO_4$ nanoparticles (Fig S7). The components at ~293.5, 292.0 and 290.2 eV in the C1s spectra clearly confirm the carbonatation of the particles (Fig. 2h), where the CO_3^{2-}/OH^- species occur not only at the surface, but also occluded in the inner volume of the $(Y_{0.95}Tb_{0.05})VO_4$ structure (Fig. 1). These results confirm that the partial carbonatation of primary vanadate grains in the colloidal synthesis culminates in vanadium-deficient solids.

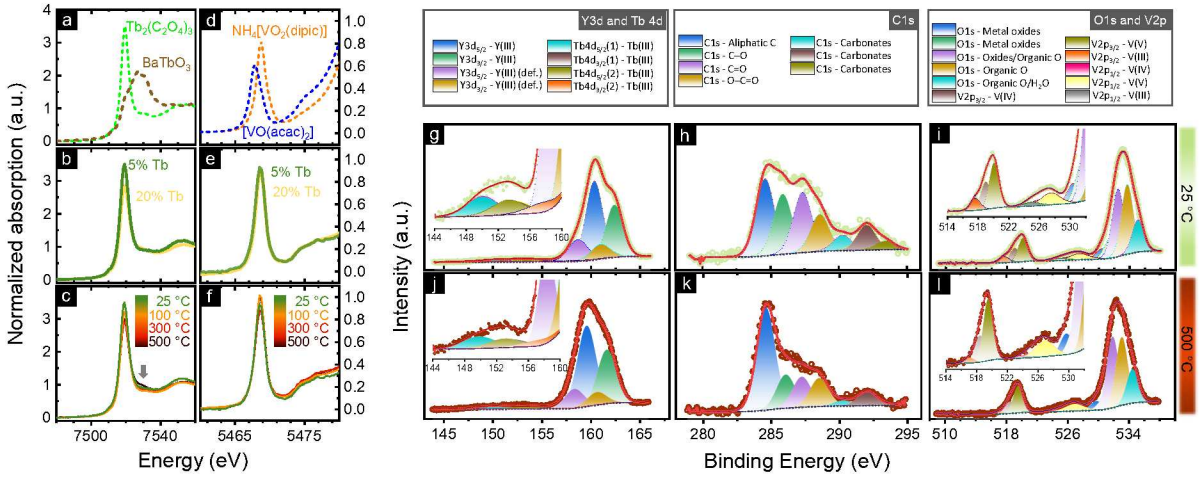

Figure 2. Tb L_{III}-edge (a-c) and V pre-K-edge (d-e) XANES spectra of (a) Tb^{3+}/Tb^{4+} and (d) V^{4+}/V^{5+} standards, (b,e) as-prepared $Y_{1-x}Tb_xVO_4$ nanoparticles (x=5% and x=20%), and (c,f) $Y_{0.95}Tb_{0.05}VO_4$ particles annealed at different temperatures. (g-l) XPS spectra of $Y_{0.95}Tb_{0.05}VO_4$ particles (g,h,i) before and (j,k,l) after annealing at 500 °C monitoring the (g,j) Y 3d and Tb 4d signals, (h,k) C 1s and (i,l) V 2p and O 1s signals. Experimental data are shown by points, and the red and dotted grey lines denote cumulative fits and backgrounds, respectively. The color legends for Voigt peaks are shown on the top.

Owing to their complex microstructure, the as-prepared $Y_{1-x}Tb_xVO_4$ particles surprisingly showed the characteristic $^5D_4 \rightarrow {}^7F_J$ Tb^{3+} emissions at 25 ˚C both under excitation at VO_4^{3-} groups (λ_{exc}=270 nm) and direct excitation at the $^5D_4$ level (λ_{exc}=488 nm, Fig. 3). As the excitation bands remained at the same energies regardless lattice constriction or expansion by substitution with Sc^{3+} or La^{3+},[38] we concluded that $VO_4^{3-} \rightarrow Tb^{3+}$ energy transfer was the only operative mechanism to afford the broadband excitation in the UV. Additional details and discussions are found in SI (Sections 6-7, p.S17-S19).

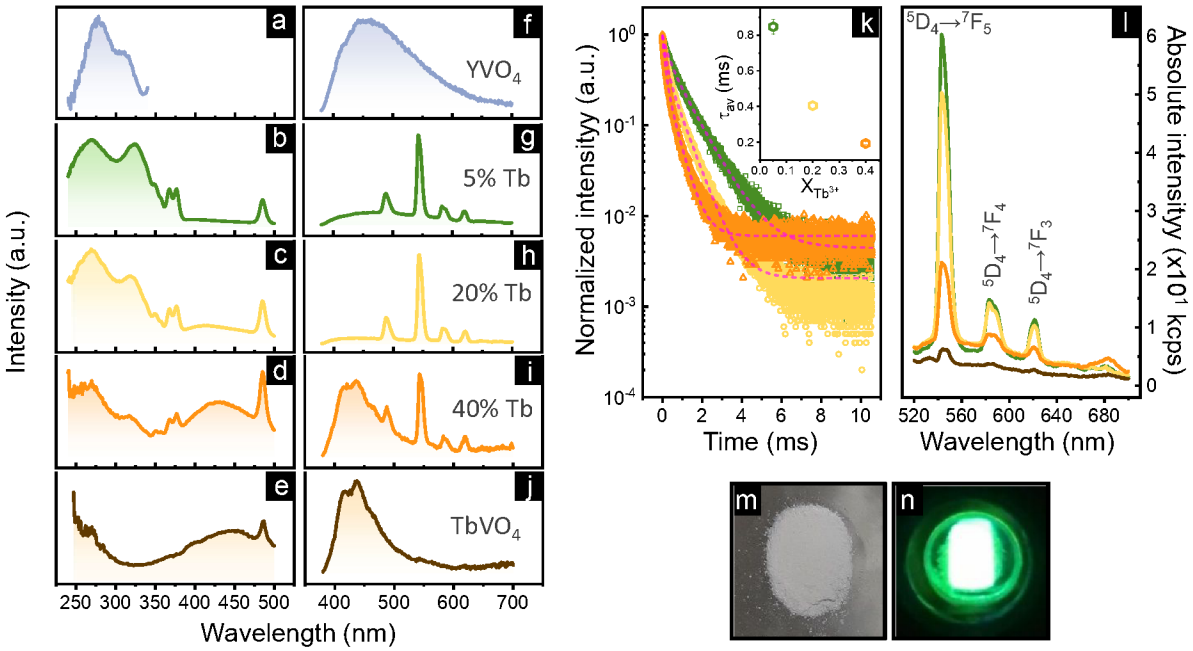

Figure 3. Photoluminescent properties of the $Y_{1-x}Tb_xVO_4$ nanoparticles (x = 0, 0.05, 0.20, 0.40, and 1). (a-e) Excitation (λ_{em} = 543 nm) and (f-j) emission (λ_{exc} = 270 nm) spectra acquired at 25 °C for the $Y_{1-x}Tb_xVO_4$ solids: (a,f) x=0, (b,g) x=0.05, (c,h) x=0.20, (d,i) x=0.40, and (e,j) x=1. (k) Tb^{3+} $^5D_4$ decay curves (λ_{exc} = 270 nm and λ_{em} = 543 nm) for the $Y_{1-x}Tb_xVO_4$ (x = 0.05, 0.20, and 0.40) solids. The inset shows average lifetimes obtained by bi-exponential fits of experimental decays as a function of the Tb^{3+} concentration. (l) Emission spectra of the $Y_{1-x}Tb_xVO_4$ (x = 0.05, 0.20, and 0.40) solids under direct excitation on the $^5D_4$ level of Tb^{3+} (λ_{exc}=488 nm). (m,n) Photographs of the $Y_{0.95}Tb_{0.05}VO_4$ powder under (m) white light and (n) UV excitation (λ_{exc} = 270 nm) at 77 K. The same color pattern for (a-j) was kept in (k) and (l).

The Tb^{3+} $^5D_4 \rightarrow {}^7F_J$ transitions [488 nm (J=6), 544 nm (J=5), 583 nm (J=4), and 622 nm (J=3)] under λ_{exc}=270 nm are superposed on the VO_4^{3-} broadband emission ($^3T_{1,2} \rightarrow {}^1A_1$), and lower Tb^{3+} concentrations led to stronger relative intensities of the *f-f* emissions (Fig. 3f-j). No signals arising from the $^5D_3$ were detected even at 77 K (Fig. S9). This is due to cross relaxation (*i.e.*, $^5D_3 + {}^7F_6 \rightarrow {}^5D_4 + {}^7F_0$) induced by the moderately high (>5%) Tb^{3+} concentrations and due to the energy position of the $^5D_3$ state, which is always above the MMCT quenching states. Nevertheless, the $^5D_4$ emissions interestingly remain detectable even at high doping concentrations (40%) where MMCT quenching should be more pronounced because of the higher probability of Tb^{4+}-V^{4+} intervalence states (Fig. 1i). The $(Y_{0.95}Tb_{0.05})VO_4$ powder particles showed a slight decrease of 7% in emission intensities after 1 h of continuous UV irradiation in air at 25 °C (Fig. S9). Photobleaching of Eu^{3+} emissions in colloidal $REVO_4$ nanoparticles has been observed due to UV-induced redox activity,[39] which in our case can be correlated to a partial oxidation of vacancies caused by irradiation in air. The reduction in the amount of oxygen defects shows a negative outcome on luminescence intensities of Tb^{3+} in YVO_4 as discussed further.

The $^5D_4$ decay curves (Fig. 3k) fitted bi-exponential functions, confirming the occupation of multiple sites at surface and lattice, as also observed for other Ln^{3+} ions in YVO_4 or different host lattices.[9,40] The $^5D_4$ lifetimes decreased at higher Tb^{3+} concentrations, in agreement with the Tb^{3+}-Tb^{3+} concentration quenching indicated by the emission spectra. Finally, literature reports that direct excitation in the $^5D_4$ emitting state is ineffective in generating Tb^{3+} luminescence in YVO_4.[25] In our case, excitation at λ_{exc}=488 nm (Fig. 3l) clearly yielded the characteristic Tb^{3+} emissions in the $Y_{1-x}Tb_xVO_4$ nanoparticles, which also demonstrates the deactivation pathways

generally reported for Tb^{3+} in YVO_4 were modified by microstructure and defect chemistry of the solids prepared herein. Hence, our results confirm not only that the $VO_4^{3-} \rightarrow Tb^{3+}$ energy transfer is operative to sensitize the Tb^{3+} luminescence in YVO_4, but also concentration quenching is more significant for the depletion of the $^5D_4$ excited state than the Tb^{4+}/V^{4+}MMCT states.

The unusual luminescent behavior of the particles obtained in this work stems from the shift of the MMCT Tb^{4+}-V^{4+} state to higher energies in comparison to YVO_4 samples prepared by conventional solid-state synthesis. So, in our case, photon absorption leads to the formation of the $^5D_4$ state by both $VO_4^{3-} \rightarrow Tb^{3+}$ energy transfer or *f-f* absorption, and radiative decay takes place instead of the $Tb^{3+} \rightarrow V^{5+}$ electron transfer. The shift in the MMCT state is caused by the nanostructural character of the $Y_{1-x}Tb_xVO_4$ particles, and by oxygen defects and RE:V non-stoichiometry induced by CO_3^{2-}/OH^- species. We therefore investigated the impact of thermal treatment on the structural and optical properties of the as-prepared particles to describe how annealing correlates to the deactivation of Tb^{3+} luminescence in YVO_4 (experimental details are described in the Supporting Information). Firstly, the $Y_{1-x}Tb_xVO_4$ particles maintained the typical tetragonal structure of YVO_4 upon heating up to 500 °C (Fig. S11), and a progressive decrease in the amount of OH^- and CO_3^{2-} groups was also detected (Fig. S12). The elimination of CO_3^{2-} at 500 °C was also detectable by the reduction of peak intensities of oxidized carbon species at high binding energies in the C1s XPS spectra (Fig. 2k). Refinement of lattice parameters against XRD data (Fig. S13) confirmed the as-prepared $Y_{0.95}Tb_{0.05}VO_4$ particles displayed expanded unit cells with a low axial ratio (*c/a*) of the tetragonal structure, as a

consequence of the nanosized crystalline coherence length, high strain, and increased number of dangling bonds at the surface.[9,41,42] Thermal treatment of these particles promoted the constriction of unit cells and decrease of the tetragonal anisotropy (*i.e.*, *c*/*a* ratio closer to 1) with the reduction of unit cell dimensions in the [100] and [010] directions. Tb L_{III}-edge XANES spectra of $Y_{0.95}Tb_{0.05}VO_4$ (Fig. 2c) after heating at 500 °C in air suggest formation of minor Tb^{4+} amounts, as indicated by the shoulder at 7528 eV in agreement with the Tb^{4+} standard (*i.e,* perovskite-type $BaTbO_3$, Fig. 2a). Although Tb^{4+} is *per se* a luminescence killer for Tb^{3+},[43] the progressive quenching of Tb^{3+} emissions upon heating cannot be ascribed to the presence of these minor amounts only. The V K-edge spectra (Fig. 2f) of the $Y_{0.95}Tb_{0.05}VO_4$ retained the profile of the as-prepared sample, and a slight displacement of the pre-edge peak from 5468.57 eV (25 °C) to 5468.62 eV (500 °C) suggested the increase in the average oxidation state of vanadium from +4.80 to +4.86 (Fig. S5). Hence, annealing in air of the $Y_{1-x}Tb_xVO_4$ particles slightly decreased the amount of electron rich vanadium sites due to oxygen abstraction. These results are also supported by V2p and Y3d XPS spectra (Fig. 2j-l, Fig. S6), which confirmed not only the oxidation of V^{3+} and formation of more V^{5+} sites, but also a decrease in the amount of Y^{3+} sites bound to oxygen defects at the surface. In summary, annealing the $Y_{1-x}Tb_xVO_4$ particles up to 500 °C in air induced two opposite trends concerning the density of defects. On the one hand, oxygen vacancies ($v_O^{\cdot\cdot}$) are generated upon heating due to condensation of OH groups [$2OH_O^{\cdot} \rightarrow O_O^x + v_O^{\cdot\cdot} + H_2O(g)$] or evolution of molecular O_2 [$O_O^x \rightarrow v_O^{\cdot\cdot} + 2e' + 1/2O_2(g)$],[9] both compensated by reduced vanadium species (V_V'). Decomposition of CO_3^{2-} species into $CO_2(g)$ further generates oxygen ($v_O^{\cdot\cdot}$) and vanadium (v_V'''') vacancies [*i.e.*, $C_V' + 2O_O^x \rightarrow 2v_O^{\cdot\cdot} + v_V'''' + CO_2(g)$, assuming carbonates occupy vanadate-like sites]. At the same time, the thermal treatment in air induces oxygen abstraction [$1/2O_2(g) + 2e' + v_O^{\cdot\cdot} \rightarrow O_O^x$], as well as crystallite

growth and decrease in the tetragonal anisotropy. The balance of these effects results in the decrease in the number of electron-rich metal sites and in the reduction of unit cell volumes.

Comparison of absorption and emission spectra of undoped YVO_4 and $Y_{0.95}Tb_{0.05}VO_4$ samples provides additional insights on the effects of the annealing on the electronic structure of the particles (Fig. S14-S15, Fig 4a). Undoped YVO_4 showed a red shift of the UV absorption edge, which is generally ascribed to V^{4+} sites and lattice $v_O^{\cdot\cdot}$ defects.[9,41,42,44,45] Although the amount of V^{4+} defects probed by XPS is approximately constant (Fig. 2 and Fig. S6), the constriction of the unit cell favors more covalent V-O bonds, which culminates in a general decrease of the energy of the V-centered states. This is also consistent with the red shift of the $^3T_{1,2}\rightarrow{}^1A_1$ emissions of VO_4^{3-} in undoped YVO_4 with increasing annealing temperatures (Fig. S15). The $Y_{0.95}Tb_{0.05}VO_4$ particles showed an additional low energy band in the absorption spectra (Fig. S14), which is due to the MMCT state. Deconvolution of the absorption spectra confirmed a progressively larger spectral contribution of this MMCT state (Fig. S16, Table S3), which becomes lower in energy with increasing calcination temperature. Consequently, the $^5D_4\rightarrow{}^7F_J$ transitions in the emission spectra (Fig. 4a) become less intense with respect to the $^3T_{1,2}\rightarrow{}^1A_1$ emissions of VO_4^{3-} for calcined samples due to the quenching of the $^5D_4$ emitting level by the Tb^{4+}-V^{4+} MMCT state. Heat-treatment in N_2 atmosphere of $Y_{0.95}Tb_{0.05}VO_4$ particles induced elimination of CO_3^{2-}/OH^- species and formation of oxygen vacancies without competitive abstraction of O_2. Indeed, absorption spectra of $Y_{0.95}Tb_{0.05}VO_4$ particles annealed in N_2 (Fig. S17) revealed increased contribution of the V^{4+}/oxygen defect band at lower energies. Interestingly, the barycenter of the Tb^{4+}-V^{4+} MMCT state of the particles annealed at 500 ˚C was higher in energy for particles

annealed in N_2 (Table S3) in comparison to the particles annealed in air. Consequently, the $^5D_4 \rightarrow {}^7F_J$ transitions in $Y_{0.95}Tb_{0.05}VO_4$ were stronger when the samples were annealed in N_2, but further treatment in air led to a more prominent quenching of the Tb^{3+} emissions (Fig. 4b). It is worth noting that even if $Y_{0.95}Tb_{0.05}VO_4$ powder annealed in N_2 showed intensified $^5D_4 \rightarrow {}^7F_J$ transitions in comparison to the treatment in air, these peaks are significantly lower in comparison to as-prepared $Y_{0.95}Tb_{0.05}VO_4$ particles. Therefore, the quenching efficiency of the $^5D_4$ level by the Tb^{4+}-V^{4+} MMCT states depends on the opposite effects of the density of $v_O^{\cdot\cdot}$ defects and of the structural alterations (*i.e.* cell constriction) induced by the thermal treatment.

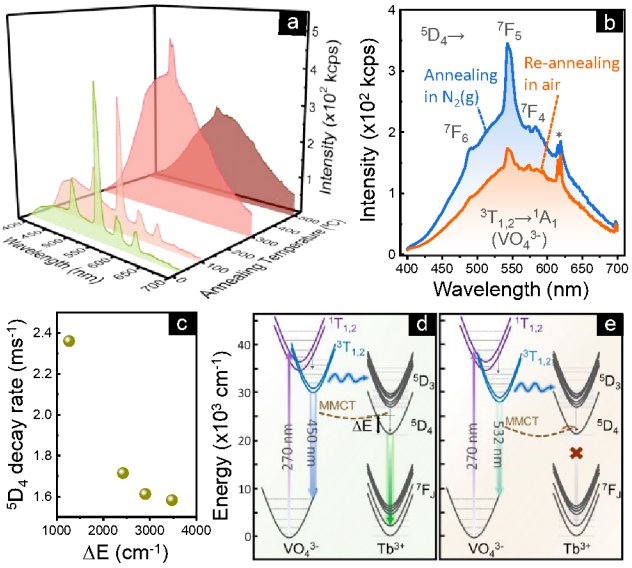

Figure 4. Emission spectra (λ_{exc} = 270 nm) of the (a) $Y_{0.95}Tb_{0.05}VO_4$ solid obtained at room temperature (25 °C) and after heat-treatments at 100, 300, and 500 °C under air atmosphere. (b) Emission spectra (λ_{exc} = 270 nm) of a $Y_{0.95}Tb_{0.05}VO_4$ sample heat-treated at 500 °C under N_2

atmosphere (blue), and of the same sample re-annealed at 500 ˚C in air (orange). Spectra in (a) and (b) were acquired at 25 ˚C. (c) Variation of the total decay rate of the $^5D_4$ state calculated from luminescence decay curves (Fig. S18) as a function of the energy separation (ΔE) between the barycenter of the Tb^{4+}-V^{4+} MMCT state (Table S3) and the minimum of the $^5D_4$ state (20492 cm^{-1}). (d,e) Illustration of the mechanisms involved in the emissions of the Tb^{3+}-doped YVO_4 solid: (d) as-prepared and low-temperature treated particles show $^5D_4$ emissions due to the high value of ΔE (>~3000 cm^{-1}); (e) the luminescence is quenched via the heat-treatment through to elimination of CO_3^{2-}/OH^- species and decrease of cell volumes, making the MMCT state to lie at lower energies. The asterisk in (b) refers to a $^5D_0 \rightarrow {}^7F_2$ line owing to a minor Eu^{3+} contamination in the $Y_{0.95}Tb_{0.05}VO_4$ annealed in N_2.

We demonstrated that the energy of the barycenter of the MMCT states (Fig S16, Table S3) probed by the absorption spectra can be directly correlated to the quenching of the $^5D_4$ emitting state in the $Y_{1-x}Tb_xVO_4$ particles (Fig. 4c). Considering the total decay rates of the $^5D_4$ level in $Y_{0.95}Tb_{0.05}VO_4$ calculated from luminescence lifetimes (Fig. S18), the energy difference (ΔE) between the minimum of the $^5D_4$ emitting level (*ca.* 20492 cm^{-1}) and the barycenter of the Tb^{4+}-V^{4+} MMCT state must be larger than ~3000 cm^{-1} to overcome the quenching induced by this charge transfer process. Therefore, the luminescence of Tb^{3+} in YVO_4 appears to be quenched when the MMCT states lies at energy differences lower than 3000 cm^{-1} with respect to the $^5D_4$

state (Fig. 4c-e). However, contrary to the results reported to date, the position of the Tb^{4+}-V^{4+} MMCT state in the yttrium vanadate nanoparticles is demonstrated to be tunable with respect to compositional and structural parameters without mixing vanadium and other pentavalent ions (*e.g.* P, As, Nb, Ta). Firstly, larger donor(Tb^{3+})-acceptor(V^{5+}) distances increase the energy barrier for the electron transfer.[46] Secondly, the presence of oxygen vacancies ($v_O^{\cdot\cdot}$) is compensated by higher electron densities on the cation sites, but this effect is greater for the V^{5+} ions covalently bound to O^{2-} than for the Tb^{3+} ions with highly ionic interactions. Hence, the increase in the electron density of the acceptor also raises the energy barrier for the $Tb^{3+}\rightarrow V^{5+}$ electron transfer. In our case, as-prepared $Y_{1-x}Tb_xVO_4$ nanoparticles showed expanded unit cells, high $v_O^{\cdot\cdot}$ densities induced by CO_3^{2-} (*i.e.*, $\frac{1}{2}v_O^{\cdot\cdot}$ compensating C_V'), and high concentrations of reduced vanadium centers induced by OH^- groups (*i.e.*, V_V' compensating $OH_O^{\cdot}$). In addition, because Tb_Y^X/C_V' pairs are not susceptible to electron transfer, the presence of CO_3^{2-} in the vicinity of Tb^{3+} centers further increases the energy barrier for the MMCT state. These factors culminate in a Tb^{4+}-V^{4+} MMCT state at particularly high energies ($\Delta E \sim 3500\ cm^{-1}$) and in a less efficient intervalence quenching. Consequently, the Tb^{3+} luminescence becomes active via $VO_4^{3-}\rightarrow Tb^{3+}$ energy transfer in the $Y_{1-x}Tb_xVO_4$ nanoparticles (Fig. 4d) even at high Tb^{3+} concentrations (x=0.40).

Thermal treatment of the materials results in unit cell contraction, reducing the donor-acceptor distances and increasing the probability of charge transfer. The decrease in the tetragonal anisotropy upon annealing due to the contraction in the [100] and [010] directions and expansion in the [001] direction (Fig. S13) indicates that the probability of electron transfer is highly dependent on V-O-Tb moieties with metal-oxygen-metal angles close to 180° (Fig. S19).

Therefore, thermal treatments remove lattice distortions of the as-prepared $Y_{1-x}Tb_xVO_4$ nanoparticles, bringing donor-acceptor pairs closer in the [100] and [010] directions where the Tb-O-V angle is ~180°, thus decreasing the energy of the Tb^{4+}-V^{4+} MMCT state. This suggests a significant role of the O^{2-} bridging anions and bond angles for the $Tb^{3+} \rightarrow V^{5+}$ charge transfer process, which is similar to observations concerning the efficiency of resonant energy transfer from excited VO_4^{3-} to Ln^{3+} ions.[47] Furthermore, annealing in air eliminates the CO_3^{2-}/OH^- species and increases the mean oxidation state of vanadium centers due to oxygen abstraction. Thus, vanadium centers become better electron acceptors and more oxygen bridges are introduced, reducing the energy of the MMCT state. Although annealing in N_2 increases the density of $v_{\ddot{O}}$ defects, this effect is partially balanced by the contraction of the unit cell, resulting in an intermediate efficiency of Tb^{3+} emission.

In summary, we described in detail for the first time the luminescence of Tb^{3+} in the YVO_4 host lattice. We demonstrated that defect-induced Tb^{3+} luminescence in YVO_4 is possible for nanosized particles synthesized at mild conditions. The commonly reported absence of Tb^{3+} luminescence in YVO_4 is due to a low-lying Tb^{4+}-V^{4+} MMCT quenching of the $^5D_4$ state, but we showed that the energy of this charge transfer state can be increased by modifying structural and compositional parameters of the YVO_4 lattice without other pentavalent metals replacing vanadium. The UV-excited luminescence of $^5D_4$ state is detectable even at high Tb^{3+} doping (40%) and in the presence high amounts of OH oscillators provided the Tb^{4+}-V^{4+} MMCT state occurs at high energies. The results obtained herein demonstrate that the radiative decay of the $^5D_4$ state of Tb^{3+} in YVO_4 will overcome the MMCT quenching if energy separations between these states are larger than ~3000 cm^{-1}. This can be achieved by synthesizing YVO_4 particles with expanded unit cells and with high tetragonal anisotropy. Increased densities of oxygen

vacancies and the presence of CO_3^{2-}/OH^- impurities also contribute to MMCT states at higher energies. Further experimental work is necessary to investigate systematically the impact of the concentration of carbonates/hydroxides on the energy of MMCT states, which can be performed by using uncarbonated metavanadates as precursors to produce intentionally carbonated YVO_4 particles with controlled amounts of CO_3^{2-}/OH^- in the reaction mixture. Our results will also motivate the investigation of Tb^{3+} luminescence on YVO_4 particles synthesized via other mild liquid-phase techniques. This opens interesting perspectives to tune YVO_4:Tb^{3+} particles aiming at new applications of the optical and (photo)redox properties of Tb^{3+} for thermal and chemical luminescent sensing.

ASSOCIATED CONTENT

Supporting Information. Additional experimental details, X-ray diffractograms, FTIR, XPS, and XANES spectra, DLS distributions of hydrodynamic diameters, additional absorption and luminescence spectra. This material is available free of charge via Internet at https://pubs.acs.org.

AUTHOR INFORMATION

Corresponding author

*Email: pcsfilho@unicamp.br. Department of Inorganic Chemistry, Institute of Chemistry, University of Campinas (Unicamp), R. Monteiro Lobato, 270, 13083-970, Campinas, São Paulo, Brazil.

ORCID

Paulo C. de Sousa Filho: 0000-0002-9210-4506

Richard I. Walton: 0000-0001-9706-2774

Notes

The authors declare no competing financial interests.

ACKNOWLEDGMENTS

The authors acknowledge the agencies CAPES, CNPq, FAEPEX-PrP-Unicamp, and FAPESP (Proc. 2017/19909-0 RVP, 2020/10518-0 PCdSF) for financial support and scholarships, and SPRINT-FAPESP (2018/08334-9) and University of Warwick for international collaboration

funding. The authors are grateful to Prof. F. Galembeck (inct-INOMAT/Unicamp) for the use of TEM instrumentation. We thank Diamond Light Source for provision of beamtime for XANES as part of the Energy Materials Block Allocation Group SP14239, and we are grateful to Professor Alan Chadwick and Dr Giannantonio Cibin for help with data acquisition. Some of the equipment used in this work was provided by the University of Warwick's Research Technology Platforms.

REFERENCES

1. Blasse, G.; Grabmaier, B. C. *Luminescent Materials*; Springer-Verlag: Berlin, 1994.

2. Lucas, J.; Lucas, P.; Le Mercier, T.; Rollat, A.; Davenport, W. *Rare Earths: Science, Technology, Production and Use*; Elsevier: Amsterdam, 2015.

3. de Sousa Filho, P. C.; Lima, J. F.; Serra, O. A. From Lighting to Photoprotection: Fundamentals and Applications of Rare Earth Materials. *J. Braz. Chem. Soc.* **2015**, *26*, 2471–2495.

4. Bünzli, J. C. G.; Eliseeva, S. V. Intriguing Aspects of Lanthanide Luminescence. *Chem. Sci.* **2013**, *4*, 1939–1949.

5. Ronda, C. C. R. *Luminescence: From Theory to Applications*; Wiley-VCH: Weinheim, 2008.

6. Shinoya, S.; Yen, W. M.; Yamamoto, H. (Eds) *Phosphor Handbook* 2nd Ed.; CRC Press: Boca Raton, 2017.

7. Jovanović, D. J. in Dhoble, S. J.; Pawade, V. B.; Swart, H. C.; Chopra, V. *Spectroscopy of Lanthanide-Doped Oxide Materials*, Elsevier, 2020. Chapter 6: Lanthanide-doped orthovanadate phosphors: Syntheses, structures, and photoluminescence properties, pp.235-291.

8. Perrella, R. V.; de Sousa Filho, P. C. High-Sensitivity Dual UV/NIR-Excited Luminescence Thermometry by Rare Earth Vanadate Nanoparticles. *Dalton Trans.* **2020**, *49*, 911–922.

9. Guida, G.; Huband, S.; Walker, M.; Walton, R. I.; de Sousa Filho, P. C. Tuning Morphology, Surface, and Nanocrystallinity of Rare Earth Vanadates by One-Pot Colloidal Conversion of Hydroxycarbonates. *Nanoscale* **2021**, *13*, 4931-4945.

10. Blasse, G. Classical Phosphors: A Pandora's Box. *J. Lumin.* **1997**, *72–74*, 129–134.

11. Ropp, R. C. Spectra of Some Rare Earth Vanadates. *J. Electrochem. Soc.* **1968**, *115*, 940–945.

12. Palilla, F. C.; Levine, A. K.; Rinkevics, M. Rare Earth Activated Phosphors Based on Yttrium Orthovanadate and Related Compounds. *J. Electrochem. Soc.* **1965**, *112*, 776–779.

13. Blasse, G.; Bril, A. Investigations of Tb^{3+}-Activated Phosphors. *Philips Res. Rep.* **1967**, *22*, 481–504.

14. Blasse, G.; Bril, A. Photoluminescent Efficiency of Phosphors with Electronic Transitions in Localized Centers. *J. Electrochem. Soc.* **1968**, *115*, 1067-1075.

15. Faria, S.; Palumbo, D. T. The Luminescence of YVO_4:Dy, YVO_4:Dy,Eu, and YVO_4:Dy,Tb. *J. Electrochem. Soc.* **1969**, *116*, 157-158.

16. Zhang, S.; Wang, L.; Peng, H.; Li, G.; Chen, K. Influence of P-doping on the Morphologies and Photoluminescence Properties of $LaVO_4$:Tb^{3+} Nanostructures. *Mater. Chem. Phys.* **2010**, *123*, 714-718.

17. Shinho, S. Synthesis and Luminescence Properties of $LaVO_4$:RE^{3+} (RE = Sm, Eu, Tb, Tm) Phosphors. *J. Nanosci. Nanotech.* **2013**, *13*, 7546-7550.

18. Dhanya, C. R.; Jeyaraman, J.; Janeesh, P. A.; Shukla, A.; Sivakumar, S.; Abraham, A. Bio-Distribution and in vivo/in vitro Toxicity Profile of PEGylated Polymer Capsules Encapsulating $LaVO_4:Tb^{3+}$ Nanoparticles for Bioimaging Applications. *RSC Adv.* **2016**, *6*, 55125-55134.

19. Jeyaraman, J.; Shukla, A.; Sivakumar, S. Targeted Stealth Polymer Capsules Encapsulating Ln^{3+}-Doped $LaVO_4$ Nanoparticles for Bioimaging Applications. *ACS Biomater. Sci. Eng.* **2016**, *2*, 1330–1340.

20. Krumpel, A. H.; van der Kolk, E.; Cavalli, E.; Boutinaud, P.; Bettinelli, M.; Dorenbos, P. Lanthanide 4f-Level Location in $AVO_4:Ln^{3+}$ (A = La, Gd, Lu) Crystals. *J. Phys. Condens. Matter* **2009**, *21*, 115503 (1-8).

21. Jeyaraman, J.; Malecka, A.; Billimoria, P.; Shukla, A.; Marandi, B.; Patel, P. M.; Jackson, A. M.; Sivakumar, S. Immuno-Silent Polymer Capsules Encapsulating Nanoparticles for Bioimaging Applications. *J. Mater. Chem. B* **2017**, *5*, 5251-5258.

22. Han, S.; Tao, Y.; Du, Y.; Yan, S.; Chen, Y.; Chen, D. Luminescence Behavior of $GdVO_4$:Tb Nanocrystals in Silica Glass-Ceramics. *Crystals* **2020**, *10*, 396 (1-12).

23. Yang, L.; Peng, S.; Zhao, M.; Yu, L. New Synthetic Strategies for Luminescent $YVO_4:Ln^{3+}$ (Ln = Pr, Sm, Eu, Tb, Dy, Ho, Er) with Mesoporous Cell-like Nanostructure. *Opt. Mater. Express* **2018**, *8*, 3805–3819.

24. Faria, S.; Mehalchick, E. J. YVO_4:Eu,Tb-An Efficient High Pressure Mercury Vapor Lamp Phosphor. *J. Electrochem. Soc.* **1974**, *121*, 305–307.

25. DeLosh, R. G.; Tien, T. Y.; Gibbons, E. F.; Zacmanidis, P. J.; Stadler, H. L. Strong Quenching of Tb^{3+} Emission by Tb-V Interaction in YPO_4-YVO_4. *J. Chem. Phys.* **1970**, *53*, 681–685.

26. Motloung, S. J.; Shaat, S. K. K.; Tshabalala, K. G.; Ntwawborwa, O. M. Structure and Photoluminescent Properties of Green-Emitting Terbium-doped $GdV_{1-x}P_xO_4$ Phosphor Prepared by Solution Combustion Method. *Luminescence* **2016**, *31*, 1069-1076.

27. Wujczyk, M.; Watras, A.; Boutinaud, P.; Betinelli, M.; Targonska, S. Hölsä, J.; Wiglusz, R. J. Emission Quenching and First Evidence of Tb^{3+}-to-As^{5+} Charge Transfer in Terbium(III) Ion-Doped $YV_xAs_{1-x}O_4$ Solid-State Solution. *J. Phys. Chem. C* **2020**, *124*, 17364-17371.

28. Blasse, G.; Bril, A. Luminescence Phenomena in Compounds with Fergusonite Structure. *J. Lumin.* **1970**, *3*, 109–131.

29. Draai, W. T.; Blasse, G. Energy Transfer from Vanadate to Rare-earth Ions in Calcium Sulphate. *Phys. Status Solidi* **1974**, *21*, 569–579.

30. Blasse, G.; Sabbatini, N. The Quenching of Rare-Earth Ion Luminescence in Molecular and Non-Molecular Solids. *Mater. Chem. Phys.* **1987**, *16*, 237–252.

31. Boutinaud, P.; Putaj, P.; Mahiou, R.; Cavalli, E.; Speghini, A.; Betinelli, M. Quenching of Lanthanide Emission by Intervalence Charge Transfer in Crystals Containing Closed Shell Transition Metal Ions. *Spectrosc. Lett.* **2007**, *40*, 209-220.

32. Stefanska, J.; Chrunik, M.; Marciniak, L. Sensitivity Enhancement of the Tb^{3+}-Based Single Band Ratiometric Luminescent Thermometry by the Metal-to-Metal Charge Transfer Process. *J. Phys. Chem. C* **2021**, *125*, 5226–5232.

33. Huignard, A.; Gacoin, T.; Boilot, J.-P. Synthesis and Luminescence Properties of Colloidal YVO_4:Eu Phosphors. *Chem. Mater.* **2000**, *12*, 1090–1094.

34. de Sousa Filho, P. C.; Gacoin, T.; Boilot, J.-P.; Walton, R. I.; Serra O. A. Synthesis and Luminescent Properties of $REVO_4$–$REPO_4$ (RE = Y, Eu, Gd, Er, Tm, or Yb) Heteronanostructures: A Promising Class of Phosphors for Excitation from NIR to VUV. *J. Phys. Chem. C* **2015**, *119*, 24062–24074.

35. Fleury, B.; Neouze, M.-A.; Guigner, J. M.; Menguy, N.; Spalla, O.; Gacoin, T.; Carriere, D. Amorphous to Crystal Conversion as a Mechanism Governing the Structure of Luminescent YVO_4:Eu Nanoparticles. *ACS Nano* **2014**, *8*, 2602–2608.

36. Neouze, M.-A.; Freitas, A. P.; Ramamoorthy, R.-K.; Mohammedi, R.; Larquet, E.; Tusseau-Nenez, S.; Carrière, D.; Gacoin, T. Toward a Chemical Control of Colloidal YVO_4 Nanoparticles Microstructure. *Langmuir* **2020**, *36*, 9124–9131.

37. Kim, H.; Jeong, H.; Byeon, S. H. Selective Filter Effect Induced by Cu^{2+} Adsorption on the Fluorescence of a $GdVO_4$:Eu Nanoprobe. *ACS Appl. Mater. Interfaces* **2016**, *8*, 15497–15505.

38. Qin, X.; Liu, X.; Huang, W.; Bettinelli, M.; Liu, X. Lanthanide-Activated Phosphors Based on 4f-5d Optical Transitions: Theoretical and Experimental Aspects. *Chem. Rev.* **2017**, *117*, 4488–4527.

39. Maksimchuk, P. O.; Hubenko, K. O.; Grygorova, G. V.; Seminko, V. V.; Bespalova, I. I.; Sorokin, A. V.; Yefimova, S. L. Photobleaching of $LnVO_4$:Eu^{3+} Nanoparticles Under UV-Light Irradiation: Effect of Nanoparticle Size. *J. Lumin.* **2022**, *242*, 118593.

40. van Hest, J. J. H. A.; Blab, G. A.; Gerritsen, H. C.; de Mello Donegá, C.; Meijerink, A. Probing the Influence of Disorder on Lanthanide Luminescence Using Eu-Doped $LaPO_4$ Nanoparticles. *J. Phys. Chem. C* **2017**, *121*, 19373-19382.

41. Yang, L.; Li, G.; Hu, W.; Zhao, M.; Sun, L.; Zheng, J.; Yan, T.; Li, L. Control over the Crystallinity and Defect Chemistry of YVO_4 Nanocrystals for Optimum Photocatalytic Property. *Eur. J. Inorg. Chem.* **2011**, *2011*, 2211–2220.

42. Yang, L.; Li, G.; Zhao, M.; Zeng, J.; Guan, X.; Li, L. Preparation and Morphology-Sensitive Luminescence Properties of Eu^{3+}-doped YVO_4: a Defect Chemistry Viewpoint of Study. *CrystEngComm* **2012**, *14*, 3227-3235.

43. Ueda, K.; Shimizu, Y.; Nagamizu, K.; Matsuo, M.; Honma, T. Luminescence and Valence of Tb Ions in Alkaline Earth Stannates and Zirconates Examined by X-Ray Absorption Fine Structures. *Inorg. Chem.* **2017**, *56*, 12625–12630.

44. Nobe, Y.; Takashima, H.; Katsumata, T. Decoloration of Yttrium Orthovanadate Laser Host Crystals by Annealing. *Opt. Lett.* **1994**, *19*, 1216–1218.

45. Garces, N. Y.; Stevens, K. T.; Foundos, G. K.; Halliburton, L. E. Electron Paramagnetic Resonance and Optical Absorption Study of V^{4+} Centres in YVO_4 Crystals. *J. Phys. Condens. Matter* **2004**, *16*, 7095–7106.

46. Setlur, A. A.; Shiang, J. J. Quantitative Analysis of Electron Transfer between $Ce^{3+}(5d^1)$ and Yb^{3+}/Eu^{3+} Ions in $Y_3Al_5O_{12}$ and $Lu_2Si_2O_7$. *J. Phys. Chem. C* **2010**, *114*, 2792–2798.

47. Jia, C. N.; Sun, L. D.; Yan, Z. G.; Pang, Y. C.; Lü, S. Z.; Yan, C. H. Monazite and Zircon Type $LaVO_4$:Eu Nanocrystals - Synthesis, Luminescent Properties, and Spectroscopic Identification of the Eu^{3+} Sites. *Eur. J. Inorg. Chem.* **2010**, 2626–2635.

TOC GRAPHICS

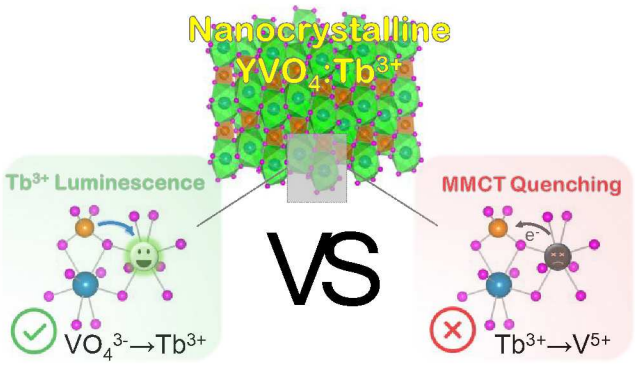

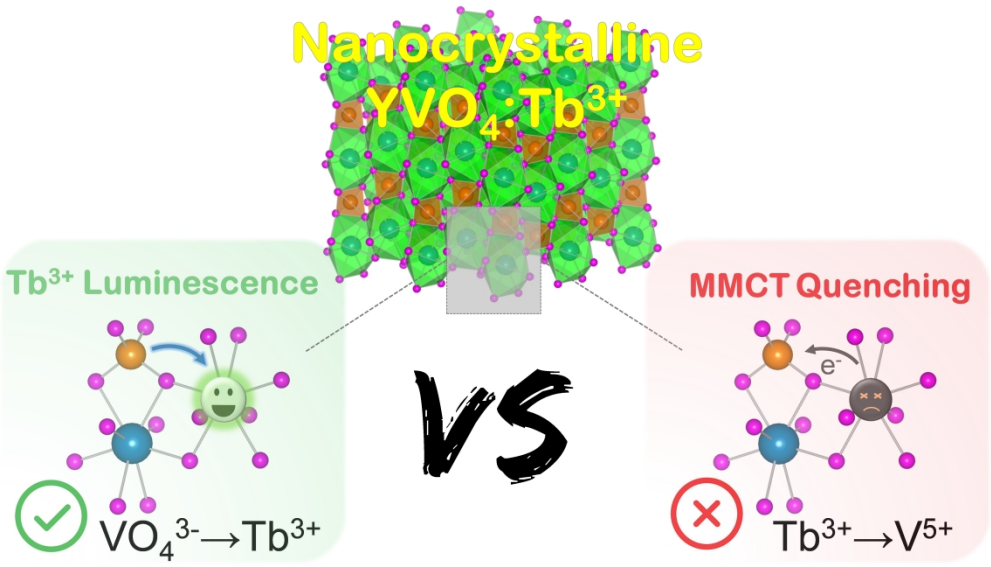

1454x821mm (96 x 96 DPI)